BIOCHEMISTRY
including biophysical chemistry & molecular biology
Article

Biochemistry **2010,** *49,* 493–501 493
DOI: 10.1021/bi9018829

Hydrogen Bond Interactions of the Pheophytin Electron Acceptor and Its Radical Anion in Photosystem II As Revealed by Fourier Transform Infrared Difference Spectroscopy†

Yuichi Shibuya,‡ Ryouta Takahashi,‡ Tatsunori Okubo,‡ Hiroyuki Suzuki,‡ Miwa Sugiura,§ and Takumi Noguchi*,‡

‡*Institute of Materials Science, University of Tsukuba, Tsukuba, Ibaraki 305-8573, Japan and* §*Cell-Free Science and Technology Research Center, Ehime University, Matsuyama, Ehime 790-8577, Japan*

Received November 3, 2009; Revised Manuscript Received December 9, 2009

ABSTRACT: The primary electron acceptor pheophytin ($Pheo_{D1}$) plays a crucial role in regulation of forward and backward electron transfer in photosystem II (PSII). It is known that some cyanobacteria control the $Pheo_{D1}$ potential in high-light acclimation by exchanging the D1 proteins from different copies of the *psbA* genes. To clarify the mechanism of the potential control of $Pheo_{D1}$, we studied the hydrogen bond interactions of $Pheo_{D1}$ in the neutral and anionic states using light-induced Fourier transform infrared (FTIR) difference spectroscopy. FTIR difference spectra of $Pheo_{D1}$ upon its photoreduction were obtained using three different PSII preparations, PSII core complexes from *Thermosynechococcus elongatus* possessing PsbA1 as a D1 subunit (PSII-PsbA1), those with PsbA3 (PSII-PsbA3), and PSII membranes from spinach. The D1-Gln130 side chain, which is hydrogen bonded to the 13^1-keto C=O group of $Pheo_{D1}$ in PSII-PsbA1, is replaced by Glu in PSII-PsbA3 and spinach PSII. The spectrum of PSII-PsbA1 exhibited 13^1-keto C=O bands at 1682 and 1605 cm^{-1} in neutral $Pheo_{D1}$ and its anion, respectively, while the corresponding bands were observed at frequencies lower by 1−3 and 18−19 cm^{-1}, respectively, in the latter two preparations. This larger frequency shift in $Pheo_{D1}^-$ than $Pheo_{D1}$ by the change of the hydrogen bond donor was well reproduced by density functional theory (DFT) calculations for the Pheo models hydrogen bonded with acetamide and acetic acid. The DFT calculations also exhibited a higher redox potential for Pheo reduction in the model with acetic acid than that with acetamide, consistent with previous observations for the D1-Gln130Glu mutant of *Synechocystis*. It is thus concluded that a stronger hydrogen bond effect on the $Pheo^-$ anion than the neutral Pheo causes the shift in the redox potential, which is utilized in the photoprotection mechanism of PSII.

Photosystem II (PSII)[1] is a multimeric protein complex that functions as a water−quinone oxidoreductase. Most of redox cofactors are bound to the reaction center complex that consists of the D1 and D2 subunits (*1*). Light illumination to PSII triggers charge separation which eventually leads to the formation of a radical pair between the special pair chlorophyll P680 and the pheophytin electron acceptor attached to the D1 subunit ($Pheo_{D1}$) (*2*). On the electron donor side, $P680^+$ oxidizes the Mn cluster through Y_Z (D1-Tyr161), and two water molecules are converted into a oxygen molecule and four protons (*3*), while on the electron acceptor side, an electron is transferred from $Pheo_{D1}$ to the primary quinone electron acceptor Q_A and then to the secondary quinone acceptor Q_B (*4*). When Q_B is doubly reduced, it is protonated and released from the protein pocket as a quinol molecule.

The $Pheo_{D1}$ plays a crucial role in regulation of forward and backward electron transfers. As a primary electron acceptor, the redox potential for one-electron reduction of $Pheo_{D1}$ (E_{red}) determines the driving force of initial charge separation and hence its quantum yield (*5*−*7*). The E_{red} of $Pheo_{D1}$ also affects the yields of recombination pathways from the charge-separated states between the Mn cluster and the quinone electron acceptors (*7*−*9*), which are closely related to photodamage and photoprotection of PSII (*10*).

The X-ray structures of PSII core complexes of cyanobacteria exhibited that D1-Gln130 is located at a hydrogen bond distance from the 13^1-keto C=O group of $Pheo_{D1}$ (*11*−*13*) (Figure 1A). Indeed, the presence of a hydrogen bond interaction at the keto C=O group was demonstrated by site-directed mutations of the amino acid residue at D1-130 in *Synechocystis* sp. PCC6803 or *Chlamydomonas reinhardtii* through monitoring the Q_x absorption band (*5*) and the g_x value of a high-field EPR spectrum (*14*). It has also been shown that hydrogen bonding at the 13^1-keto C=O group affects the E_{red} of $Pheo_{D1}$ (*6*−*8*). Replacement of the D1-Gln130 with Leu and Glu in *Synechocystis* induced E_{red} shifts by −50−56 and +30−39 mV, respectively, as estimated by time-resolved absorption (*6*) and thermoluminescence (*8*) measurements. The higher E_{red} of $Pheo_{D1}$ increased a charge recombination rate (*8*, *9*) and decreased the rate of photodamage of PSII (*15*).

Thermosynechococcus elongatus has three copies of *psbA* genes, each of which encodes a different D1 protein isoform. Under normal culture conditions with a relatively low light intensity (~40 μmol m^{-2} s^{-1}) and optimum temperatures (55−60 °C), *psbA1* is mainly expressed as a D1 subunit (*16*). Under high-light

†This study was supported by Grants-in-Aid for Scientific Research from the Ministry of Education, Culture, Sports, Science, and Technology (21108506, 21370063, and 17GS0314) to T.N. and Grant-in-Aid for JSPS fellows (204647) to R.T.

*To whom correspondence should be addressed. Phone: +81-29-853-5126. Fax: +81-29-853-4490. E-mail: tnoguchi@ims.tsukuba.ac.jp.

[1]Abbreviations: DFT, density functional theory; DM, *n*-dodecyl β-D-maltoside; E_{red}, redox potential of one-electron reduction of pheophytin; EA, electron affinity; FTIR, Fourier transform infrared; IR, infrared; Pheo, pheophytin; $Pheo_{D1}$, redox-active pheophytin attached to the D1 protein in photosytem II; PSII, photosystem II; P680, the special pair chlorophyll of photosystem II; Q_A, primary quinone electron acceptor; Q_B, secondary quinone electron acceptor; SHE, standard hydrogen electrode.

Published on Web 12/09/2009

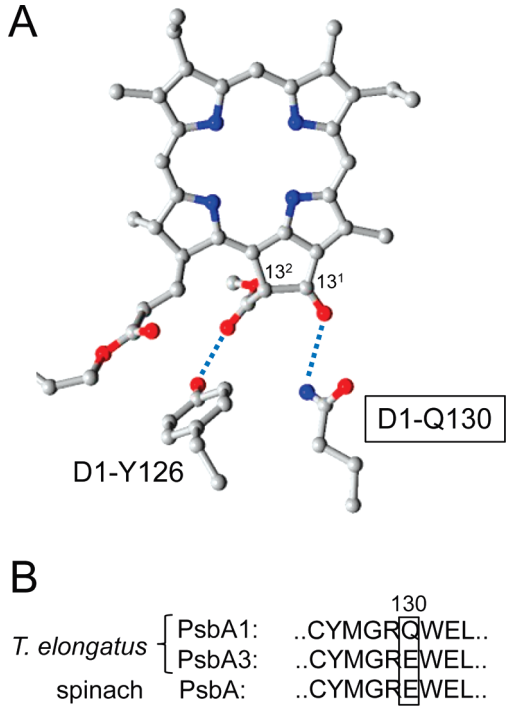

FIGURE 1: (A) Structure and hydrogen bond interactions of $Pheo_{D1}$ in the X-ray crystallographic structure of the PSII core complex from *T. elongatus* (*12*). In this PSII complex, the *psbA1* gene is expressed as the D1 protein (*17*). (B) Sequence alignment of the PsbA (D1) protein around the amino acid residue at D1-130 in *T. elongatus* (PsbA1 and PsbA3) and spinach.

conditions, however, PsbA3 replaces the PsbA1 protein, while the transcript level of the *psbA2* gene remains at a trace level (*16*). PsbA1 has D1-Gln130, whereas the Gln is replaced by Glu in PsbA3 as well as in the PsbA proteins of higher plants (Figure 1B) (*16*−*18*). This amino acid change, which induces the E_{red} shift of $Pheo_{D1}$, was attributed to the accelerated rates of charge recombination from $S_2Q_A^-$ and $S_2Q_B^-$ in high-light acclimated cells of *T. elongatus* (*16*), although the degree of acceleration was smaller than that observed in the above site-directed mutants of *Synechocystis* (*8*, *9*). Similar regulation of *psbA* gene expression under different light conditions has also been reported in other cyanobacteria such as *Synechococcus* sp. PCC7942 (*19*, *20*). Thus, the *psbA* regulation to control the $Pheo_{D1}$ potential seems to be an acclimation mechanism that functions in some species of cyanobacteria.

To understand the mechanism of the redox potential regulation of $Pheo_{D1}$, it is essential to directly monitor the presence and the strength of the hydrogen bond at the keto C=O group in both neutral and anionic states of $Pheo_{D1}$ in PSII preparations. In this study, we investigated the correlation between the E_{red} of Pheo and the hydrogen bond strengths of the 13^1-keto C=O group of neutral Pheo and its radical anion using light-induced Fourier transform infrared (FTIR) difference spectroscopy and density functional theory (DFT) calculations. Light-induced FTIR difference spectroscopy has been used as a powerful technique to detect the structure and interactions of redox cofactors in photosynthetic proteins (*21*−*23*). FTIR difference spectra of $Pheo_{D1}$ upon its photoreduction ($Pheo_{D1}^-/Pheo_{D1}$ spectra) were previously obtained using PSII particles and isolated reaction centers of higher plants (*24*, *25*). In this study, we compared the $Pheo_{D1}^-/Pheo_{D1}$ FTIR spectra of three different PSII preparations: PSII core complexes from *T. elongatus* possessing the PsbA1 protein as a D1 subunit, those with the PsbA3 protein, and PSII-enriched membranes from spinach. The former preparation with PsbA1 has D1-Gln130, whereas the latter two preparations have D1-Glu130. The FTIR results along with the DFT analysis for Pheo models hydrogen bonded with acetamide and acetic acid showed that a stronger hydrogen-bonding effect on the keto C=O group in a $Pheo^-$ anion than in a neutral Pheo causes the E_{red} shift upon alteration of a hydrogen bond donor.

MATERIALS AND METHODS

T. elongatus 43H (*26*) and WT* (*27*) strains were grown in DNT medium at 45 °C under continuous light with an intensity of ~60 μmol m^{-2} s^{-1} (*26*, *27*). PSII core complexes were purified from *T. elongatus* cells as described previously (*26*) and suspended in a pH 6.0 buffer involving 10 mM Mes, 5 mM NaCl, and 0.06% DM. After Mn depletion by 10 mM NH_2OH treatment at room temperature (*26*), the sample was concentrated to ~4.5 mg of Chl/mL using Microcon-100 (Amicon). PSII-enriched membranes of spinach were prepared following the method previously described (*28*) and suspended in a pH 6.5 buffer involving 40 mM Mes, 400 mM sucrose, and 20 mM NaCl. Mn depletion was performed by 10 mM NH_2OH treatment (*29*). The Mn-depleted PSII membranes were suspended in a buffer diluted 40 times with water, and the sample was concentrated to ~5 mg of Chl/mL by centrifugation.

For FTIR measurements, an aliquot of the suspension of Mn-depleted PSII core complexes of *T. elongatus* (9 μL of ~4.5 mg of Chl/mL) or spinach PSII membranes (10 μL of ~5 mg of Chl/mL) was deposited on a BaF_2 plate (13 mm in diameter) and lightly dried under N_2 gas flow. The sample was then sandwiched with another BaF_2 plate together with 1 μL (for core complexes) or 2 μL (for membranes) of 1 M sodium dithionite solution.

The sample temperature was adjusted to 210 K in a cryostat (Oxford DN1704) using a controller (Oxford ITC-4). Light-induced FTIR spectra were recorded on a Bruker IFS-66/S spectrophotometer equipped with an MCT detector (D313-L) at 4 cm^{-1} resolution. $Pheo_{D1}^-/Pheo_{D1}$ difference spectra were obtained by recording single-beam spectra for 150 s (300 scans) before and after illumination for 30 s by continuous white light (~40 mW/cm^2 at the sample surface) from a halogen lamp (Sigma Koki PHL-150). Measurements were repeated three times for the core samples to obtain averaged spectra. In this case, during the interval of measurements, the sample was warmed to 283 K to relax the $Pheo_{D1}^-$ anion and then cooled again to 210 K. For PSII membranes, one difference spectrum was measured for each sample, and two spectra were averaged.

Molecular orbital calculations were performed using the Gaussian03 program package (*30*). The initial structure of the Pheo model was adopted from the X-ray structure of $Pheo_{D1}$ in PSII (*12*). Hydrogen atoms were added to this structure, and the 17-phytyl ester group was replaced with a methyl group. In hydrogen-bonded Pheo models, acetamide and acetic acid were chosen as hydrogen bond donors to the 13^1-keto C=O group. The B3LYP functional (*31*, *32*) with the 6-31+G(d) basis set was used to optimize the geometries of the Pheo models in both neutral and anionic forms and to calculate the electronic energies, vibrational frequencies, and IR intensities for the optimized structures. All calculations were done in the gas phase. The calculated vibrational frequencies were scaled with a scaling factor of 0.9640. When the vibrations of acetamide and acetic acid were strongly coupled to the 13^1-keto C=O vibration of

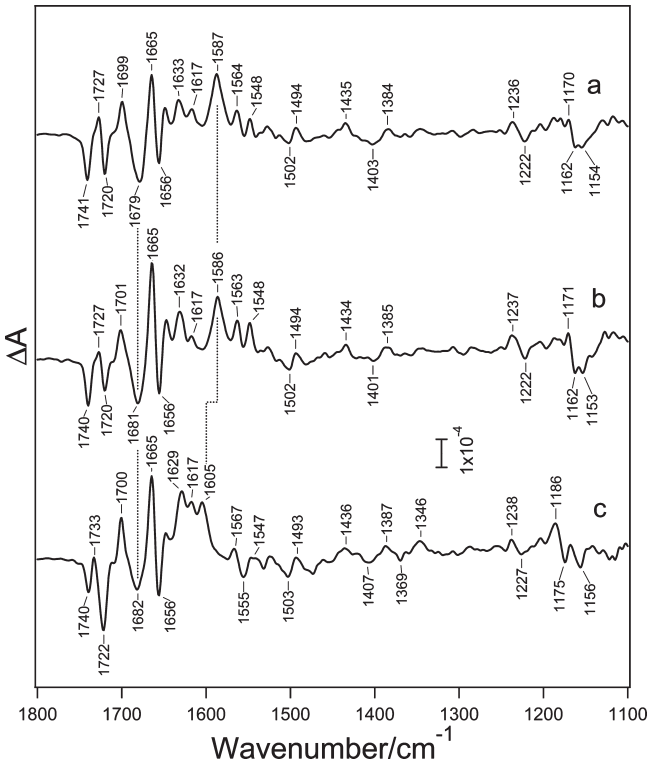

FIGURE 2: Light-induced $Pheo_{D1}^{-}/Pheo_{D1}$ FTIR difference spectra of PSII membranes from spinach (a) and PSII core complexes from *T. elongatus* including PsbA3 (b) and PsbA1 (c) as the D1 protein.

Pheo, such coupling was removed by appropriate isotope substitution in these hydrogen bond donors. Electron affinity (EA) of Pheo was calculated by subtracting the sum of electronic and zero-point energies of the anionic form from that of the neutral form. The redox potential for Pheo reduction versus the standard hydrogen electrode (SHE) was calculated by the equation:

$$E_{red} = EA - 4.43$$

where the value of 4.43 eV is an estimate of the absolute potential of SHE (*33*, *34*).

RESULTS

$Pheo_{D1}^{-}/Pheo_{D1}$ FTIR Difference Spectra. Three PSII preparations were used for FTIR measurements of $Pheo^{-}/Pheo$ difference spectra: PSII-enriched membranes from spinach and two types of PSII core complexes from different strains of *T. elongatus*, i.e., the 43H strain (*26*) in which the carboxyl terminus of the CP43 subunit was genetically His-tagged and the WT* strain (*27*) in which the *psbA1* and *psbA2* genes were deleted in addition to His tagging of CP43. While spinach has only a single *psbA* gene, *T. elongatus* has three *psbA* copies, *psbA1*, *psbA2*, and *psbA3*. The 43H strain possesses all of the three *psbA* genes but mainly expresses the *psbA1* gene to encode the D1 protein under normal growth conditions (*16*, *17*), whereas the D1 protein of the WT* strain originates solely from the *psbA3* gene. The PSII core preparations from the former and latter strains of *T. elongatus* are designated hereafter as PSII-PsbA1 and PSII-PsbA3, respectively.

Figure 2a shows a light-induced $Pheo_{D1}^{-}/Pheo_{D1}$ FTIR difference spectrum of the PSII membranes from spinach. This spectrum is very similar to the corresponding spectra previously obtained using spinach PSII particles and the D1/D2 reaction center complexes from pea by Nabedryk and co-workers (*24*, *25*). The neutral $Pheo_{D1}$ and the $Pheo_{D1}^{-}$ anion provide negative and positive peaks, respectively, which are superimposed by the bands of protein moieties perturbed by $Pheo_{D1}$ reduction.

Nabedryk et al. (*25*) provided assignments of some bands in the $Pheo_{D1}^{-}/Pheo_{D1}$ spectrum by comparison with a redox-induced $Pheo^{-}/Pheo$ difference spectrum in THF solution. The prominent negative band at 1679 cm^{-1} (1677 cm^{-1} in ref *25*) was assigned to the 13^1-keto C=O stretching bands of neutral $Pheo_{D1}$ hydrogen bonded to D1-Glu130. Previous resonance Raman spectra of $Pheo_{D1}$ also reported the keto C=O band at similar frequencies of 1680−1679 cm^{-1} (*35*, *36*). Although Nabedryk et al. did not explicitly assign the prominent positive peak at 1587 cm^{-1}, the observation of a large downshift of the keto C=O peak from 1706 to 1656 cm^{-1} upon Pheo reduction in THF (*25*) suggests the assignment of this peak to the 13^1-keto C=O vibration of the $Phoe_{D1}^{-}$ anion. The bands at 1741/1727 and 1720/1699 cm^{-1} should arise from the C=O stretches of either the 13^2-ester C=O group of $Pheo_{D1}$ or a carboxylic acid group that typically shows a band in the 1760−1700 cm^{-1} region. Nabedryk et al. (*25*) assigned the negative peaks at 1741 and 1720 cm^{-1} (1739 and 1721 cm^{-1} in their spectrum) to the D1-Glu130 side chain, which engages a hydrogen bond with the keto C=O group, and to the 13^2-ester C=O group of $Pheo_{D1}$, respectively. A strong differential signal at 1665/1656 cm^{-1} is probably due to the amide I vibrations, which reflect some perturbations in the polypeptide main chains around $Pheo_{D1}$ upon its reduction. Medium and weak peaks below 1633 cm^{-1} may mostly arise from the chlorin ring vibrations of $Pheo_{D1}$ in the neutral and anionic forms.

The $Pheo_{D1}^{-}/Pheo_{D1}$ spectrum of the PSII-PsbA3 core complexes of *T. elongatus* (Figure 2b) showed features virtually identical to those of spinach PSII membranes (Figure 2a). The frequencies of all appreciable peaks agree with each other within 2 cm^{-1}, and their relative intensities are also almost the same. In sharp contrast, the spectrum of the PSII-PsbA1 complexes of *T. elongatus* (Figure 2c) showed features significantly different from the spectra of the former two preparations. The most prominent change is a large upshift of the strong keto C=O peak of $Pheo^{-}$ from 1587−1586 to 1605 cm^{-1} by 18−19 cm^{-1} (Figure 2, dotted line). The absence of the 1586 cm^{-1} peak in PSII-PsbA1 confirms that *psbA3* was little expressed in the *T. elongatus* 43H strain under the culture condition used in this study. The corresponding negative peak of the keto C=O of neutral $Pheo_{D1}$, however, showed only a slight upshift by 1−3 cm^{-1} from 1681−1679 to 1682 cm^{-1}. Another prominent change is an intensified negative peak at 1722 cm^{-1} in PSII-PsbA1 concomitant with a slight frequency upshift. The negative peak at 1740 cm^{-1} was instead slightly weakened, and the corresponding positive peak was upshifted from 1727 to 1733 cm^{-1}. The spectral features in the 1570−1100 cm^{-1} region also somewhat changed; the peaks at 1564−1563, 1403−1401, 1385−1384, 1222, 1171−1170, 1162, and 1154−1153 cm^{-1} upshifted by several wavenumbers to 1567, 1407, 1387, 1227, 1186, 1175, and 1156 cm^{-1}, respectively.

The spectral differences in the C=O stretching region are more clearly expressed in the expanded spectra in Figure 3, in which the spectra of the spinach PSII (Figure 3a, red line) and the *T. elongatus* PSII-PsbA3 (Figure 3b, red line) are overlaid on the spectrum of PSII-PsbA1 (Figure 3a, b, black lines). Double difference spectra between spinach PSII and PSII-PsbA1 and between PSII-PsbA3 and PSII-PsbA1 are also shown in Figure 3c and Figure 3d, respectively. In these double difference spectra (Figure 3c,d), prominent differential signals at 1605/1587−1585 cm^{-1} correspond to the shifts of the 13^1-keto C=O bands

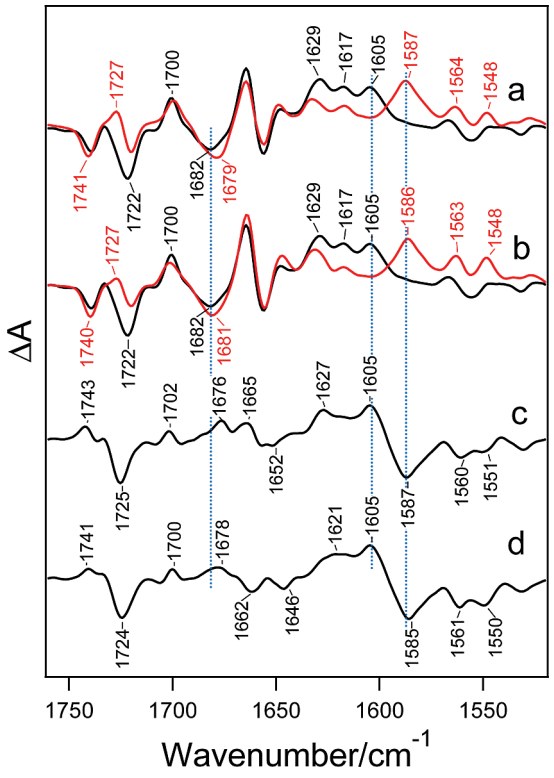

FIGURE 3: (a, b) The C=O stretching region of the Phe_{D1}^-/$Pheo_{D1}$ FTIR difference spectra of spinach PSII membranes (a, red line) and *T. elongatus* PSII core complexes with PsbA3 (b, red line) in comparison with the spectrum of *T. elongatus* PSII core complexes with PsbA1 (black lines). (c, d) Double difference spectra between the two spectra in panel a (PsbA1 minus spinach) (c) and those in panel b (PsbA1 minus PsbA3) (d).

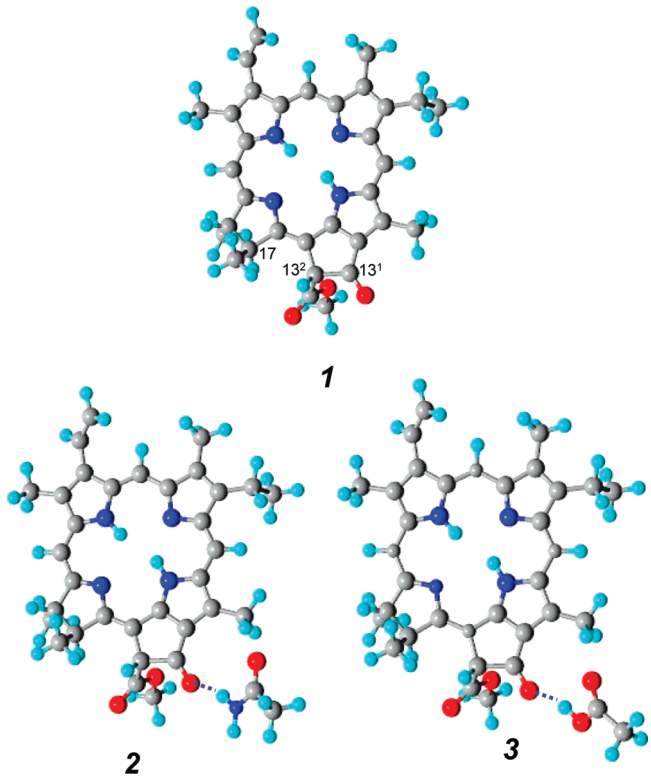

FIGURE 4: Optimized geometries of Pheo models in the neutral forms obtained by DFT calculations. The Pheo models, in which the 17-phytyl ester group is replaced with a methyl group, are free from hydrogen bonding (model 1) and hydrogen bonded with acetamide (model 2) and acetic acid (model 3) at the 13^1-keto C=O group. Gray, blue, red, and cyan balls represent carbon, nitrogen, oxygen, and hydrogen atoms, respectively.

of the $Pheo_{D1}^-$ anion (Figure 3a,b). Spectral changes in the 1750−1720 cm^{-1} region were expressed as positive and negative peaks at 1743−1741 and 1725−1724 cm^{-1}, respectively, in the double difference spectra. Notably, the latter negative signal was much stronger than the former positive signal. Slight shifts and intensity changes in the 13^1-keto C=O bands of neutral $Pheo_{D1}$ around 1680 cm^{-1} are expressed as a broad positive feature at 1678−1676 cm^{-1} in the double difference spectra. Some intensity change in the bands at 1629, 1617, 1564−1563, and 1548 cm^{-1} (Figure 3a,b) are shown as positive and negative features around 1625 and 1555 cm^{-1}, respectively, in both double difference spectra (Figure 3c,d). Weak features in the 1665−1640 cm^{-1} region, which are somewhat different between the two double difference spectra, may arise from the amide I bands that are sensitive to preparations and sample conditions.

DFT Calculations of Pheo Models. Electronic energies and vibrational frequencies of neutral Pheo and its radical anion were calculated using the DFT method at the B3LYP/6-31+G(d) level. In addition to free Pheo (model 1), two Pheo models hydrogen bonded at the 13^1-keto C=O group with acetamide (model 2) and acetic acid (model 3) were used for calculation, mimicking $Pheo_{D1}$ hydrogen bonded with Gln and Glu side chains, respectively. The optimized geometries of these models in the neutral forms are shown in Figure 4. Calculated normal-mode frequencies of Pheo and $Pheo^-$ (without the modes of hydrogen bond donors) in the 1750−1500 cm^{-1} region are presented in Tables S1 and S2 (Supporting Information), respectively, together with the IR intensities. All frequencies were scaled with a scaling factor of 0.9640 to adjust the calculated 13^1-keto C=O frequency of free Pheo to the experimental value of 1706 cm^{-1} in THF (*25*).

The estimated 13^1-keto C=O frequencies are collected in Table 1 together with experimental values. In model 2 (with acetamide) and model 3 (with acetic acid), the keto C=O frequencies in the neutral forms were estimated to be 1683 and 1679 cm^{-1}, respectively, which are lower than the frequency of free Pheo by 23 and 27 cm^{-1}. These keto C=O frequencies are in good agreement with the experimental values of 1682 and 1681−1679 cm^{-1} in PSII with D1-Gln130 (PSII-PsbA1) and that with D1-Glu130 (PSII-PsbA3 and spinach PSII), respectively. Upon reduction of free Pheo, the calculated keto C=O frequency exhibited a large downshift of 63 cm^{-1}, reasonably consistent with the observed downshift of 50 cm^{-1} in THF (*25*). The C=O frequencies of the $Pheo^-$ anion in model 2 and model 3 were estimated to be 1610 and 1592 cm^{-1}, respectively, providing reduction-induced downshifts of 73 and 87 cm^{-1}, in good agreement with the observed downshifts of 77 and 92−95 cm^{-1}, respectively. The frequency differences between model 2 and model 3 are 4 and 18 cm^{-1} in neutral and anionic forms, respectively, which also agree well with the observed differences of 1−3 and 18−19 cm^{-1} between PSII with D1-Gln130 and that with D1-Glu130.

Using the calculated normal-mode frequencies and IR intensities, $Pheo^-$/Pheo IR difference spectra in the 1750−1500 cm^{-1} region were calculated as sums of Gaussian bands with widths of 10 cm^{-1} for model 2 (Figure 5a, blue line) and model 3 (Figure 5a, red line). Note that these calculated spectra do not include bands of hydrogen bond donors, acetamide and acetic

Table 1: Experimental and Calculated 13^1-Keto C=O Stretching Frequencies (cm^{-1}) of Pheophytin and Its Radical Anion

samples or calcd models[a]	H-bond donor[b]	neutral[c]	anion[c]	anion − neutral
experimental				
THF solution[d]	none	1706	1656	−50
T. elongatus PSII-PsbA1	glutamine	1682	1605	−77
T. elongatus PSII-PsbA3	glutamic acid	1681	1586	−95
spinach PSII	glutamic acid	1679	1587	−92
calculated				
model 1	none	1706	1643	−63
model 2	acetamide	1683	1610	−73
model 3	acetic acid	1679	1592	−87

[a]Optimized geometries of the calculated models in the neutral forms are presented in Figure 4. [b]Hydrogen bond donor to the 13^1-keto C=O. [c]All calculated frequencies were scaled with a scaling factor of 0.9640 to adjust the C=O frequency of free neutral Pheo (model 1) to the experimental value of 1706 cm^{-1} in THF (*25*). [d]Data from Nabedryk et al. (*25*).

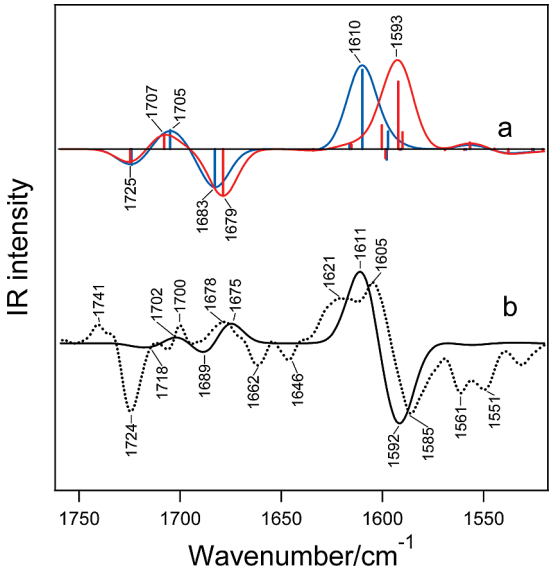

FIGURE 5: (a) Calculated $Pheo^-$/Pheo infrared difference spectra of model 2 (blue line) and model 3 (red line), in which the 13^1-keto C=O group is hydrogen bonded with acetamide and acetic acid, respectively. The intensities of individual vibrations in Pheo and $Pheo^-$ are expressed with negative and positive bars, respectively, from the zero line. The spectra were calculated as sums of Gaussian bands with a bandwidth of 10 cm^{-1}. (b) A calculated double difference spectrum (model 2 minus model 3, solid line) in comparison with the experimental double difference spectrum (PsbA1 minus PsbA3, dotted line) after appropriate scaling.

acid. Strong positive bands at 1610 and 1593 cm^{-1} for model 2 and model 3, respectively, arise from the 13^1-keto C=O vibrations of the $Pheo^-$ anion with some overlaps of the CC stretching bands of the 3-vinyl group and the chlorin ring (Table S2, Supporting Information), while negative bands at 1683 and 1679 cm^{-1} of model 2 and model 3, respectively, arise solely from the 13^1-keto C=O vibrations of neutral Pheo. The negative and positive bands at 1725 and 1707−1705 cm^{-1} originate from the 13^2-ester C=O vibrations of neutral Pheo and its anion, respectively. Although the calculated 13^2-ester C=O frequencies are a little too low compared with the observed ones in THF (1743 and 1728 cm^{-1} in Pheo and $Pheo^-$, respectively), the downshift upon reduction by 18−20 cm^{-1} is consistent with the observed downshift of 15 cm^{-1}.

Using these calculated difference spectra (Figure 5a), the double difference spectrum between model 3 and model 2 was

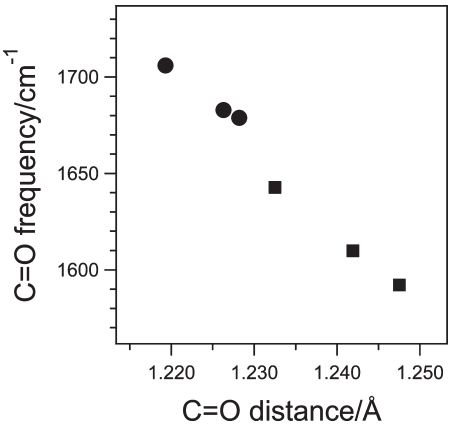

FIGURE 6: Relationship between the calculated distances and stretching frequencies of the 13^1-keto C=O bonds in the Pheo models. Solid circles and solid squares represent neutral and anionic states, respectively.

calculated (Figure 5b, solid line). The large positive and negative bands at 1611 and 1592 cm^{-1}, respectively, arise from the 13^1-keto C=O vibrations of $Pheo^-$, while the corresponding bands of neutral Pheo appear at 1689 and 1675 cm^{-1} with only weak intensities reflecting a small frequency difference in the original spectra (Figure 5a). Since the 13^2-ester C=O signal is little affected by different hydrogen-bonding interaction at the keto C=O, weaker signals of the ester C=O group are seen at 1718 and 1702 cm^{-1}. The superimposition of the observed double difference spectrum between PSII-PsbA3 and PSII-PsbA1 (Figure 5b, dotted line) shows that overall features, i.e., a prominent differential signal around 1600 cm^{-1} and weak signals around 1680 cm^{-1}, are well reproduced by the calculation. Other features that are not observed in the calculated double difference spectrum may mostly arise from amino acid and polypeptide vibrations.

Figure 6 shows the relationship between the calculated distance and stretching frequency of the 13^1-keto C=O bond. (The C=O distances are collected in Table S3 in Supporting Information.) Solid circles and solid squares represent the neutral Pheo and $Pheo^-$ anion, respectively, in the three Pheo models. It is clear that the keto C=O frequency has a linear correlation with a C=O distance irrespective of neutral and anionic states. Thus, the lower C=O frequencies in $Pheo^-$ anions are attributed to the longer C=O distances than neutral Pheo, and the hydrogen-bonding effect on the keto C=O frequency directly reflects the change in the C=O distance in either the neutral or the anionic state.

The O···H distances of the hydrogen bonds between the keto C=O and acetamide in the neutral and anionic states of model 2 are 1.979 and 1.911 Å, respectively, while the hydrogen bonds with acetic acid exhibit shorter values of 1.792 (neutral) and 1.661 (anion) Å in model 3 (Table S3, Supporting Information). Thus, acetic acid forms stronger hydrogen bonds than acetamide in both the neutral and anionic states, and the hydrogen bonds in the anion are stronger than in the neutral Pheo in both models.

The calculated electron affinity (EA) and the redox potential (E_{red}) of Pheo in the three models are summarized in Table 2. The E_{red} of free Pheo in the gas phase was estimated to be −2.479 V, which is much lower than the observed values of −0.6−0.9 V in organic solvents (*37*, *38*). This discrepancy is ascribed mainly to the dielectric constant dependence of a redox potential as previously shown in the DFT study of a chlorophyll model (*39*). Indeed, Heimdal et al. (*40*) reported a similar value of −2.58 V at

Table 2: Electron Affinities and Redox Potentials Calculated for the Pheophytin Model and Its Hydrogen-Bonded Complexes

calcd models[a]	H-bond donor[b]	EA (eV)[c]	E_{red} (V)[d]	ΔE_{red} (mV)[e]	exptl ΔE_{red} (mV)[f]
model 1	none	1.951	−2.479	0	0
model 2	acetamide	2.018	−2.412	+67	+50−56
model 3	acetic acid	2.102	−2.328	+151	+80−91

[a]Optimized geometries of the calculated models in the neutral forms are presented in Figure 4. [b]Hydrogen bond donor to the 13^1-keto C=O. [c]Electron affinities calculated from the electronic energies corrected with zero-point energies of neutral and anionic Pheo in the gas phase. [d]Redox potentials versus SHE for one-electron reduction of Pheo were calculated by E_{red} = EA − 4.43. [e]Shifts of the redox potentials by hydrogen bond formation. [f]Experimental redox potential differences between PSII preparations with D1-Leu130 (free) and those with D1-Gln130 or D1-Glu130 estimated by Merry et al. (*6*) and Cser and Vass (*8*).

ε = 1 but significantly higher values of −1.53 and −0.99 V at ε = 4 and 80, respectively, in their DFT calculations of a Pheo model. Also, Mehta and Datta (*41*) calculated the E_{red} of Pheo in *N*,*N*-dimethylformamide to be −0.9−1.0 by involving solvent effects. Thus, our estimation of E_{red} of Pheo is reasonably consistent with previous calculations and experimental data.

Upon hydrogen bond formation at the 13^1-keto C=O with acetamide (model 2) and acetic acid (model 3), E_{red} was estimated to increase by +67 and +151 mV, respectively (Table 2). Thus, Pheo hydrogen bonded with acetic acid has an E_{red} value higher than that with acetamide by +84 mV.

DISCUSSION

Detection of Hydrogen Bond Interactions in Pheo and Pheo$^-$ by Light-Induced FTIR Difference Spectroscopy. In the present study, hydrogen bond interactions of the 13^1-keto C=O group of $Pheo_{D1}$ in both neutral and anionic states in different PSII preparations were directly monitored by detecting C=O stretching frequencies using light-induced FTIR difference spectroscopy. In the $Pheo_{D1}^-/Pheo_{D1}$ difference spectra, the keto C=O bands were observed at 1605/1682 cm^{-1} in *T. elongatus* PSII-PsbA1 having D1-Gln130 and at 1587−1586/1679−1681 cm^{-1} in *T. elongatus* PSII-PsbA3 and spinach PSII having D1-Glu130 (Figure 3, Table 1). Thus, the frequencies significantly downshifted by 77−92 cm^{-1} upon anion formation in all preparations. The above C=O frequencies are also lower than those in the Pheo$^-$/Pheo spectrum of free Pheo in THF (1656/1706 cm^{-1}) (*25*) by 51−70/24−27 cm^{-1} (Table 1), indicating the presence of a hydrogen bond with D1-Gln(Glu)130 in both the neutral and anionic states. The notable observation is that the frequency is only slightly (by 1−3 cm^{-1}) lowered by replacing D1-Gln130 with Glu in the neutral $Pheo_{D1}$, whereas a significant downshift of 18−19 cm^{-1} is detected in the $Pheo_{D1}^-$ anion.

These observed shifts of the keto C=O frequencies of $Pheo_{D1}$ were well reproduced by DFT calculations for the Pheo models (Figure 4). The C=O frequencies are lowered by 63−87 cm^{-1} upon reduction and by 23−27 and 33−51 cm^{-1} by hydrogen bond formation with Pheo and Pheo$^-$, respectively (Table 1). The frequencies are downshifted by changing the hydrogen bond donor from acetamide to acetic acid by 4 and 18 cm^{-1} in the neutral and anionic states, respectively, which are comparable to the experimental values of 1−3 and 18−19 cm^{-1}. The good agreement between the experimental and theoretical results is also expressed in Figure 5b, in which the double difference spectrum between PSII-PsbA3 and PSII-PsbA1 and that between model 3 and model 2 show similar features. Such an agreement indicates that the much larger shift of the keto C=O frequency in the $Pheo_{D1}^-$ anion than in the neutral $Pheo_{D1}$ upon replacing D1-Gln130 with Glu originates purely from the chemical properties of Pheo (in neutral and anionic states) and hydrogen bond donors (amide or carboxylic acid) but is not related to spatial restriction in hydrogen bond formation often seen in proteins.

The DFT results in the present study are basically consistent with the previous DFT study by O'Malley (*42*), in which the keto C=O frequencies of free Pheo and a Pheo model hydrogen bonded with formic acid were calculated at the B3LYP/6-31G(d) level. He observed a downshift by 62 cm^{-1} upon anion formation in free Pheo, which is in good agreement with the downshift of 63 cm^{-1} in our result. The downshift by hydrogen bond formation with formic acid was 50 and 94 cm^{-1} in the neutral and anionic states, respectively, which is significantly larger than our values, 27 and 51 cm^{-1}, respectively, for the Pheo model hydrogen bonded with acetic acid. This discrepancy may be ascribed to the higher acidity of formic acid than acetic acid and the differences in the basis set (6-31G(d) vs 6-31+G(d)) and the model Pheo structure (in his Pheo model, 13^1-methyl ester and 17-phytyl ester groups were replaced with hydrogen atoms) used for the calculations. However, the tendency of a larger downshift by hydrogen bonding in Pheo$^-$ than neutral Pheo is conserved between the two studies.

The present observation of a hydrogen bond interaction between the Pheo keto C=O and D1-Glu130 indicates that this Glu side chain takes a protonated form. Thus, the C=O stretching bands of D1-Glu130 should be located in the general COOH region (1760−1700 cm^{-1} (*43*)) of the Pheo$^-$/Pheo spectra of spinach PSII and *T. elongatus* PSII-PsbA3. The negative peak at 1741−1740 cm^{-1} in these spectra (Figure 3a,b, red lines) was previously assigned to D1-Glu130 by Nabedryk et al. (*25*). However, this band only slightly decreased its intensity by replacement of D1-Glu130 with Gln in PSII-PsbA1 (Figure 3a, b, black lines), indicating that D1-Glu130 only partly contributes to this band. Double difference spectra between spinach PSII and PSII-PsbA1 (Figure 3c) and between PSII-PsbA3 and PSII-PsbA1 (Figure 3d) showed a large negative band at 1725−1724 cm^{-1} along with a small positive band at 1743−1741 cm^{-1}. Thus, the band at 1725−1724 cm^{-1} can be a candidate of D1-Glu130 interacting with the Pheo$^-$ anion. The frequency decrease by 17−18 cm^{-1} is consistent with a strengthened hydrogen bond with Pheo$^-$. The significantly stronger intensity of this band than the 1743−1741 cm^{-1} band could be due to stronger hydrogen bonding, although such a drastic intensity increase was not reproduced by the DFT calculations (data not shown). The assignment of the COOH band can be confirmed by an ∼10 cm^{-1} downshift upon deuteration. Unfortunately, however, the bands in the 1750−1700 cm^{-1} region in the Pheo$^-$/Pheo spectra of PSII-PsbA3 were almost unchanged in D_2O buffer except for only a slight downshift (∼1 cm^{-1}) of the 1740 cm^{-1} peak, in agreement with the previous observation by Nabedryk et al. (*25*). This insensitivity to D_2O is probably because of the hydrophobic environment around $Pheo_{D1}$.

A complicated situation in interpretation of the bands in 1750−1700 cm^{-1} is the possible heterogeneity of hydrogen-bonding status of the 13^2-ester C=O group. Such heterogeneity has been proposed in the bacteriopheophytin electron acceptor ($BPheo_L$) in bacterial reaction centers. Breton et al. (*44*) showed that there are different conformations in $BPheo_L$ with free and hydrogen-bonded 13^2-ester C=O group showing FTIR bands at 1747 and 1732−1725 cm^{-1}, respectively, and the population distribution of these conformations changes by mutation of L-Glu104, a hydrogen bond donor to the 13^1-keto C=O group. A similar story seems to hold for PSII. D1-Tyr126 is located within a hydrogen bond distance from the 13^2-ester C=O group in PSII (Figure 1A) (*11*−*13*). $Pheo_{D1}$ with a 13^2-ester C=O group hydrogen bonded with D1-Tyr126 gives a peak at 1722−1720 cm^{-1}, while some population of $Pheo_{D1}$ with a free 13^2-ester C=O provides a contribution to the peak at 1741−1740 cm^{-1} (Figures 2 and 3a,b). Different hydrogen-bonding interactions at the 13^1-keto C=O group will affect the population distribution of these conformations and alter the band pattern in the 1750−1700 cm^{-1} region. Definitive assignments of the 13^2-ester C=O bands as well as the D1-Glu130 bands will require further studies using mutations at D1-Tyr126.

Correlation between the Redox Potential of Pheo and the Hydrogen Bond Interaction at the 13^1-Keto C=O Group in the Neutral and Anionic States. DFT calculations of the Pheo models in the present study clearly showed the correlation between the E_{red} of Pheo and the hydrogen bond strength at the 13^1-keto C=O group. The Pheo models with acetamide (model 2) and acetic acid (model 3) provided E_{red} values higher than the free Pheo (model 1) by +67 and +151 mV, respectively (Table 2). These E_{red} shifts are comparable to the experimental values of +50−56 and +80−91 mV, respectively, deduced from the estimation of ΔE_{red} of $Pheo_{D1}$ by mutations of D1-Gln130 to Leu and Glu in *Synechocystis* sp. PCC6803 (*6*, *8*) (Table 2). The larger value in calculations than in experiments is due probably to the estimation in the gas phase ($\varepsilon = 1$), which also causes the much lower E_{red} values (−2.328−2.479 V; Table 2) than experimental ones in organic solvents (−0.6−0.9 V (*37*, *38*)). It is underlined, however, that the tendency of higher E_{red} values in the order of no hydrogen bond, a hydrogen bond with an amide group, and that with a carboxylic acid group, is well reproduced in the calculations.

The E_{red} shift by some perturbation is determined by the difference in the shift of the absolute energy between Pheo and $Pheo^-$. As shown above, $Pheo^-$ exhibits a larger C=O frequency change than neutral Pheo. This indicates that $Pheo^-$ undergoes a larger structural rearrangement than neutral Pheo upon hydrogen bond formation or the change in the hydrogen bond strength. In fact, the keto C=O frequency is linearly correlated with the C=O distance irrespective of the neutral and anionic states of Pheo (Figure 6). It is thus concluded that a stronger hydrogen-bonding effect on $Pheo^-$ than Pheo to stabilize the former to more extent is the mechanism of the E_{red} shift by the change in the keto C=O hydrogen bond.

The E_{red} of $Pheo_{D1}$ has been estimated to be −500−600 mV in plant PSII and *T. elongatus* PSII-PsbA3 (*45*−*47*), which is relatively higher than the reported E_{red} range of isolated Pheo in aprotic organic solvents (−560−900 mV (*37*, *38*)). These PSII preparations have D1-Glu130 that provides a strong hydrogen bond to the keto C=O of $Pheo_{D1}$. Hence, it is conceived that one of the factors that determines the relatively high E_{red} of $Pheo_{D1}$ is a hydrogen-bonding effect on the keto C=O group, which should increase the E_{red} by 80−90 mV compared with the free interaction, although the dielectric environments (*39*) and the charge distribution around $Pheo_{D1}$ (*48*) may also be important factors to contribute to the E_{red}.

Some cyanobacteria such as *T. elongatus* and *Synechococcus* sp. PCC7942 have a high-light acclimation mechanism in which the PsbA protein having D1-Gln130 is replaced with another PsbA isoform with D1-Glu130 (*16*, *17*, *19*, *20*). The replacement of D1-Gln130 with Glu in the D1 protein accelerates charge recombination (*7*, *9*, *16*) and decreases the rate of photodamage (*15*). Although the differences in the charge recombination rate and the thermoluminescence features between PSII-PsbA1 and PSII-PsbA3 of *T. elongatus* were relatively small (*16*, *27*) compared with those observed in site-directed mutants in which Gln and Glu are exchanged at D1−130 in *Synechocystis* PCC 6803 and *C. reinhardtii* (*7*−*9*), this may be due to some compensation effects on the cofactors involved in the recombination processes by the 20 other substitutions in PsbA1 and PsbA3 as suggested previously (*16*, *27*). Vass and Cser (*10*) attributed the PSII protection against photodamage by the D1-Gln130Glu replacement to the increase in the E_{red} of $Pheo_{D1}$ by this amino acid change. They explained that the E_{red} increase accelerates the direct recombination of $^1[P680^+Pheo^-]$ by the decrease in the energy gap between $P680^+Pheo^-$ and P680Pheo, which is in the inverted Marcus region about the charge recombination reaction, and thus prevents the formation of a harmful triplet state. The E_{red} increase by 30−40 mV upon the Gln to Glu change (*6*, *8*) is due to a stronger hydrogen-bonding effect on $Pheo_{D1}^-$ than neutral $Pheo_{D1}$ as clearly shown in the FTIR spectra and DFT estimations in the present study (Figure 3, Table 1). Thus, this type of high-light acclimation in cyanobacteria utilizes the property of Pheo in which the structure of the anionic state is more affected than that of the neutral state by the change in the hydrogen bond strength at the keto C=O group.

SUPPORTING INFORMATION AVAILABLE

Calculated normal-mode frequencies (cm^{-1}) in the 1750−1500 cm^{-1} region and the calculated distances of the 13^1-keto C=O bond and the O···H hydrogen bond of the Pheo models. This material is available free of charge via the Internet at http://pubs.acs.org.

REFERENCES

1. Nixon, P. J., Sarcina, M., and Diner, B. A. (2005) The D1 and D2 core proteins, in Photosystem II: The Light-Driven Water:Plastoquinone Oxidoreductase (Wydrzynski, T., and Satoh, K., Eds.) pp 71−94, Springer, Dordrecht, The Netherlands.
2. Renger, G., and Holzwarth, A. R. (2005) Primary electron transfer, in Photosystem II: The Light-Driven Water:Plastoquinone Oxidoreductase (Wydrzynski, T., and Satoh, K., Eds.) pp 139−175, Springer, Dordrecht, The Netherlands.
3. Hillier, W., and Messinger, J. (2005) Mechanism of photosynthetic oxygen production, in Photosystem II: The Light-Driven Water: Plastoquinone Oxidoreductase (Wydrzynski, T., and Satoh, K., Eds.) pp 567−608, Springer, Dordrecht, The Netherlands.
4. Petrouleas, V., and Crofts, A. R. (2005) The quinone iron acceptor complex, in Photosystem II: The Light-Driven Water:Plastoquinone Oxidoreductase (Wydrzynski, T., and Satoh, K., Eds.) pp 177−206, Springer, Dordrecht, The Netherlands.
5. Giorgi, L. B., Nixon, P. J., Merry, S. A. P., Joseph, D. M., Durrant, J. R., Rivas, J. D., Barber, J., Porter, G., and Klug, D. R. (1996) Comparison of primary charge separation in the photosystem II reaction center complex isolated from wild-type and D1−130 mutants of the cyanobacterium *Synechocystis* PCC 6803. *J. Biol. Chem. 271*, 2093–2101.
6. Merry, S. A. P., Nixon, P. J., Barter, L. M. C., Schilstra, M., Porter, G., Barber, J., Durrant, J. R., and Klug, D. R. (1998) Modulation of

quantum yield of primary radical pair formation in photosystem II by site-directed mutagenesis affecting radical cations and anions. *Biochemistry 37*, 17439–17447.
7. Cuni, A., Xiong, L., Sayre, R., Rappaport, F., and Lavergne, J. (2004) Modification of the pheophytin midpoint potential in photosystem II: Modulation of the quantum yield of charge separation and of charge recombination pathways. *Phys. Chem. Chem. Phys. 6*, 4825–4831.
8. Cser, K., and Vass, I. (2007) Radiative and non-radiative charge recombination pathways in photosystem II studied by thermoluminescence and chlorophyll fluorescence in the cyanobacterium *Synechocystis* 6803. *Biochim. Biophys. Acta 1767*, 233–243.
9. Rappaport, F., Guergova-Kuras, M., Nixon, P. J., Diner, B. A., and Lavergne, J. (2002) Kinetics and pathways of charge recombination in photosystem II. *Biochemistry 41*, 8518–8527.
10. Vass, I., and Cser, K. (2009) Janus-faced charge recombinations in photosystem II photoinhibition. *Trends Plant Sci. 14*, 200–205.
11. Ferreira, K. N., Iverson, T. M., Maghlaoui, K., Barber, J., and Iwata, S. (2004) Architecture of the photosynthetic oxygen-evolving center. *Science 303*, 1831–1838.
12. Guskov, A., Kern, J., Gabdulkhakov, A., Broser, M., Zouni, A., and Saenger, W. (2009) Cyanobacterial photosystem II at 2.9-Å resolution and the role of quinones, lipids, channels and chloride. *Nat. Struct. Mol. Biol. 16*, 334–342.
13. Kawakami, K., Umena, Y., Kamiya, N., and Shen, J.-R. (2009) Location of chloride and its possible functions in oxygen-evolving photosystem II revealed by X-ray crystallography. *Proc. Natl. Acad. Sci. U.S.A. 106*, 8567–8572.
14. Dorlet, P., Xiong, L., Sayre, R. T., and Un, S. (2001) High field EPR study of the pheophytin anion radical in wild type and D1-E130 mutants of photosystem II in *Chlamydomonas reinhardtii*. *J. Biol. Chem. 276*, 22313–22316.
15. Cser, K., and Vass, I. (2008) Regulation of photoprotection by non-radiative charge recombination in photosystem II, in Photosynthesis. Energy from the Sun (Allen, J. F., Gantt, E., Golbeck, J. H., and Osmond, B., Eds.) pp 47−50, Springer, Dordrecht, The Netherlands.
16. Kos, P. B., Deak, Z., Cheregi, O., and Vass, I. (2008) Differential regulation of *psbA* and *psbD* gene expression, and the role of the different D1 protein copies in the cyanobacterium *Thermosynechococcus elongatus* BP-1. *Biochim. Biophys. Acta 1777*, 74–83.
17. Loll, B., Broser, M., Kos, P. B., Kern, J., Biesiadka, J., Vass, I., Saenger, W., and Zouni, A. (2008) Modeling of variant copies of subunit D1 in the structure of photosystem II from *Thermosynechococcus elongatus*. *Biol. Chem. 389*, 609–617.
18. Svensson, B., Vass, I., and Styring, S. (1991) Sequence-analysis of the D1 and D2 reaction center proteins of photosystem II. *Z. Naturforsch. 46c*, 765–776.
19. Clarke, A. K., Soitamo, A., Gustafsson, P., and Oquist, G. (1993) Rapid interchange between two distinct forms of cyanobacterial photosystem II reaction-center protein D1 in response to photoinhibition. *Proc. Natl. Acad. Sci. U.S.A. 90*, 9973–9977.
20. Golden, S. S. (1995) Light-responsive gene-expression in cyanobacteria. *J. Bacteriol. 177*, 1651–1654.
21. Noguchi, T., and Berthomieu, C. (2005) Molecular analysis by vibrational spectroscopy, in Photosystem II: The Light-Driven Water:Plastoquinone Oxidoreductase (Wydrzynski, T., and Satoh, K., Eds.) pp 367−387, Springer, Dordrecht, The Netherlands.
22. Noguchi, T. (2007) Light-induced FTIR difference spectroscopy as a powerful tool toward understanding the molecular mechanism of photosynthetic oxygen evolution. *Photosynth. Res. 91*, 59–69.
23. Berthomieu, C., and Hienerwadel, R. (2009) Fourier transform infrared (FTIR) spectroscopy. *Photosynth. Res. 101*, 157–170.
24. Tavitian, B. A., Nabedryk, E., Mäntele, W., and Breton, J. (1986) Light-induced Fourier transform infrared spectroscopic investigations of primary reactions in photosystem I and photosystem II. *FEBS Lett. 201*, 151–157.
25. Nabedryk, E., Andrianambinintsoa, S., Berger, G., Leonhard, M., Mäntele, W., and Breton, J. (1990) Characterization of bonding interactions of the intermediary electron-acceptor in the reaction center of photosystem II by FTIR spectroscopy. *Biochim. Biophys. Acta 1016*, 49–54.
26. Sugiura, M., and Inoue, Y. (1999) Highly purified thermo-stable oxygen-evolving photosystem II core complex from the thermophilic cyanobacterium *Synechococcus elongatus* having His-tagged CP43. *Plant Cell Physiol. 40*, 1219–1231.
27. Sugiura, M., Boussac, A., Noguchi, T., and Rappaport, F. (2008) Influence of histidine-198 of the D1 subunit on the properties of the primary electron donor, P680, of photosystem II in *Thermosynechococcus elongatus*. *Biochim. Biophys. Acta 1777*, 331–342.
28. Ono, T., and Inoue, Y. (1986) Effects of removal and reconstitution of the extrinsic 33, 24 and 16 kDa proteins on flash oxygen yield in photosystem II particles. *Biochim. Biophys. Acta 850*, 380–389.
29. Noguchi, T., and Inoue, Y. (1995) Molecular interactions of the redox-active accessory chlorophyll on the electron-donor side of photosystem II as studied by Fourier transform infrared spectroscopy. *FEBS Lett. 370*, 241–244.
30. Frisch, M. J., Trucks, G. W., Schlegel, H. B., Scuseria, G. E., Robb, M. A., Cheeseman, J. R., Montgomery, J. A., Jr., Vreven, T., Kudin, K. N., Burant, J. C., Millam, J. M., Iyengar, S. S., Tomasi, J., Barone, V., Mennucci, B., Cossi, M., Scalmani, G., Rega, N., Petersson, G. A., Nakatsuji, H., Hada, M., Ehara, M., Toyota, K., Fukuda, R., Hasegawa, J., Ishida, M., Nakajima, T., Honda, Y., Kitao, O., Nakai, H., Klene, M., Li, X., Knox, J. E., Hratchian, H. P., Cross, J. B., Bakken, V., Adamo, C., Jaramillo, J., Gomperts, R., Stratmann, R. E., Yazyev, O., Austin, A. J., Cammi, R., Pomelli, C., Ochterski, J. W., Ayala, P. Y., Morokuma, K., Voth, G. A., Salvador, P., Dannenberg, J. J., Zakrzewski, V. G., Dapprich, S., Daniels, A. D., Strain, M. C., Farkas, O., Malick, D. K., Rabuck, A. D., Raghavachari, K., Foresman, J. B., Ortiz, J. V., Cui, Q., Baboul, A. G., Clifford, S., Cioslowski, J., Stefanov, B. B., Liu, G., Liashenko, A., Piskorz, P., Komaromi, I., Martin, R. L., Fox, D. J., Keith, T., Al-Laham, M. A., Peng, C. Y., Nanayakkara, A., Challacombe, M., Gill, P. M. W., Johnson, B., Chen, W., Wong, M. W., Gonzalez, C., and Pople, J. A. (2004) Gaussian 03, Revision C.02, Gaussian, Inc., Wallingford, CT.
31. Becke, A. D. (1993) Density-functional thermochemistry. III. The role of exact exchange. *J. Chem. Phys. 98*, 5648–5652.
32. Lee, C., Yang, W., and Parr, R. G. (1988) Development of the Colle-Salvetti correlation-energy formula into a functional of the electron density. *Phys. Rev. B 37*, 785–789.
33. Trasatti, S. (1986) The absolute electrode potential: An explanatory note. *Pure Appl. Chem. 58*, 955–966.
34. Reiss, H., and Heller, A. (1985) The absolute potential of the standard hydrogen electrode: A new estimate. *J. Phys. Chem. 89*, 4207–4213.
35. Moënne-Loccoz, P., Robert, B., and Lutz, M. (1989) A resonance Raman characterization of the primary electron-acceptor in photosystem II. *Biochemistry 28*, 3641–3645.
36. Germano, M., Pascal, A., Shkuropatov, A. Y., Robert, B., Hoff, A. J., and van Gorkom, H. J. (2002) Pheophytin-protein interactions in photosystem II studied by resonance Raman spectroscopy of modified reaction centers. *Biochemistry 41*, 11449–11455.
37. Kazakova, A. A., Kisselev, B. A., and Kozlov, Y. N. (1989) Electrochemical reduction of pheophytin and its participation in the functioning of photosystem II. *Bioelectrochem. Bioenerg. 21*, 367–372.
38. Watanabe, T., and Kobayashi, M. (1991) Electrochemistry of chlorophylls, in Chlorophylls (Scheer, H., Ed.) pp 287−315, CRC Press, Boca Raton, FL.
39. Hasegawa, K., and Noguchi, T. (2005) Density functional theory calculations on the dielectric-constant dependence of the oxidation potential of chlorophyll: Implication for the high potential of P680 in photosystem II. *Biochemistry 44*, 8865–8872.
40. Heimdal, J., Jensen, K. P., Devarajan, A., and Ryde, U. (2007) The role of axial ligands for the structure and function of chlorophylls. *J. Biol. Inorg. Chem. 12*, 49–61.
41. Mehta, N., and Datta, S. N. (2007) Theoretical determination of the standard reduction potentials of pheophytin-*a* in *N*,*N*-dimethyl formamide and membrane. *J. Phys. Chem. B 111*, 7210–7217.
42. O'Malley, P. J. (2000) Density functional predicted geometries and vibrational frequencies of the neutral and anion-radical form of pheophytin: Relevance to electron transfer in photosynthetic reaction centres. *Chem. Phys. Lett. 331*, 78–82.
43. Takei, K., Takahashi, R., and Noguchi, T. (2008) Correlation between the hydrogen-bond structures and the C=O stretching frequencies of carboxylic acids as studied by density functional theory calculations: Theoretical basis for interpretation of infrared bands of carboxylic groups in proteins. *J. Phys. Chem. B 112*, 6725–6731.
44. Breton, J., Bibikova, M., Oesterhelt, D., and Nabedryk, E. (1999) Conformational heterogeneity of the bacteriopheophytin electron acceptor H_A in reaction centers from *Rhodopseudomonas viridis* revealed by Fourier transform infrared spectroscopy and site-directed mutagenesis. *Biochemistry 38*, 11541–11552.
45. Klimov, V. V., Allakhverdiev, S. I., Demeter, S., and Krasnovskii, A. A. (1979) Photoreduction of pheophytin in photosystem 2 of chloroplasts with respect to redox potential of the medium. *Dokl. Akad. Nauk SSSR 249*, 227–230.
46. Rutherford, A. W., Mullet, J. E., and Crofts, A. R. (1981) Measurement of the midpoint potential of the pheophytin acceptor of photosystem II. *FEBS Lett. 123*, 235–237.

47. Kato, Y., Sugiura, M., Oda, A., and Watanabe, T. (2009) Spectroelectrochemical determination of the redox potential of pheophytin *a*, the primary electron acceptor in photosystem II. *Proc. Natl. Acad. Sci. U.S.A. 106*, 17365–17370.

48. Ishikita, H., Biesiadka, J., Loll, B., Saenger, W., and Knapp, E. W. (2006) Cationic state of accessory chlorophyll and electron transfer through pheophytin to plastoquinone in photosystem II. *Angew. Chem. 45*, 1964–1965.